

Heterogeneity in susceptibility dictates the order of epidemiological models

Christopher Rose,¹ Andrew J. Medford,² C. Franklin Goldsmith,¹
Tejs Vegge,³ Joshua S. Weitz,^{4,*} and Andrew A. Peterson^{1,3,†}

¹*School of Engineering, Brown University, Providence, Rhode Island, 02912, USA*

²*School of Chemical & Biomolecular Engineering,
Georgia Institute of Technology, Atlanta, Georgia, 30332, USA*

³*Department of Energy Conversion and Storage,
Technical University of Denmark, 2800 Kgs. Lyngby, Denmark*

⁴*School of Biological Sciences, Georgia Institute of Technology, Atlanta, Georgia, 30332, USA*

The fundamental models of epidemiology describe the progression of an infectious disease through a population using compartmentalized differential equations, but do not incorporate population-level heterogeneity in infection susceptibility. We show that variation strongly influences the rate of infection, while the infection process simultaneously sculpts the susceptibility distribution. These joint dynamics influence the force of infection and are, in turn, influenced by the shape of the initial variability. Intriguingly, we find that certain susceptibility distributions (the exponential and the gamma) are unchanged through the course of the outbreak, and lead naturally to power-law behavior in the force of infection; other distributions often tend towards these “eigen-distributions” through the process of contagion. The power-law behavior fundamentally alters predictions of the long-term infection rate, and suggests that first-order epidemic models that are parameterized in the exponential-like phase may systematically and significantly over-estimate the final severity of the outbreak.

Mathematical models of disease dynamics divide a population into categories based on infection status; *e.g.*, susceptible (S), infectious (I), and recovered/removed (R). In the basic SIR model, the dynamics of individuals in each compartment can be written as¹

$$\begin{aligned}\frac{dS}{dt} &= -r_I \\ \frac{dI}{dt} &= r_I - r_R,\end{aligned}\tag{1}$$

such that $S + I + R = 1$. The Kermack–McKendrick² formulation—the basis for conventional, modern epidemiology models—assumes rates of infection and recovery to be $r_I = \beta IS$ and $r_R = \gamma I$, respectively, with β and γ taken as rate constants with dimensions of inverse time. These simplified models provide epidemiologists and policymakers with valuable intuition on the progression of an outbreak, and form the basis for more complex models that include such effects as geography, travel, latency, susceptibility to re-infection, stochasticity, and vital dynamics.^{3–6} Previous studies have explored nonlinear forms for the rate of infection, r_I ; many forms have been suggested including power laws and sub-exponential growth.^{7–12}

The SIR model assumes homogeneity of risk, an assumption unlikely to hold in practice. That is, a real population will have a distribution of susceptibilities which can be based on a mixture of behavioral attributes (such as the number of people encountered in a typical day or interaction modalities) and inherent attributes (such as age, immune status, genetic differences, or varied responses to vaccines).^{13–20} Here, we confine our analysis to the simplest case where individuals have a static susceptibility, noting that dynamic changes in behavior can be accounted for separately.²¹ While measurement

of susceptibilities is certainly not straightforward, most studies suggest that a small percentage of the population carries a majority of the population’s total susceptibility.^{16,18,20,22,23} If there is variation, then individuals that are more susceptible should tend to be infected earlier, leading to changes in the susceptibility distribution. As a result, the most susceptible individuals will be disproportionately removed from the pool at the early stages of an outbreak, so that not just the *number* of people in the susceptible pool will decrease, but also the *average susceptibility* of the pool will decrease, both of which should slow the rate of spread of infections.

One way to incorporate variability into the SIR model is to directly account for susceptibility in the rate equations. Other epidemic models have incorporated such variability by explicitly accounting for assortative mixing²⁴ or variation in contacts,²⁵ by implicitly structuring a population based on variation in susceptibility,²⁶ or by the use of network-based models.²⁷ These analyses make different assumptions about the link between variation in risk and infection dynamics. Despite the use of different assumptions, all of these models suggest that variation in the risk of transmission can lower the herd immunity threshold (*i.e.*, the fraction of the population that must become immune for the disease to decrease in prevalence) when compared to predictions from equivalent homogeneous mixing models. This agreement suggests it may be possible to develop a unified framework to understand the joint dynamics of infection and susceptibility.

Here, we define an individual’s infection susceptibility, ε , such that individuals with $\varepsilon=2$ will become infected at twice the rate, on average, as individuals with $\varepsilon=1$, given they exist in the same population of infected people. This definition is generic, and captures heterogeneity

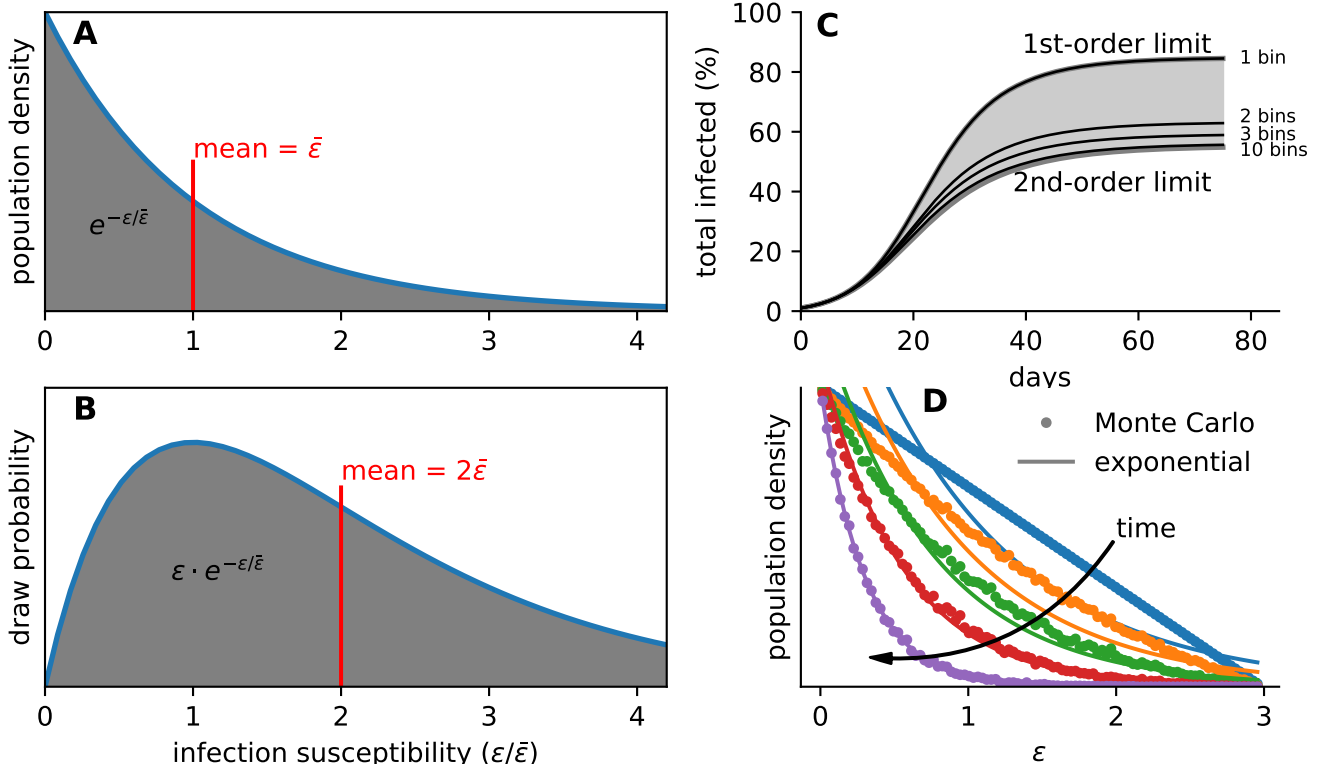


FIG. 1: **A** and **B** show a continuous distribution of infection susceptibility in a population and the probability of the next individual infected, respectively. For an exponential distribution, the mean of the lower curve is double the mean of the upper curve. **C** compares numerically integrating a 1st- and 2nd-order SIR model with that obtained from binning the susceptibility into discrete levels consistent with an initially-exponential distribution. **D** shows that an exponential distribution emerges when stochastically sampling from an initially linear distribution. The solid lines are exponential curves with the same mean as the Monte Carlo points of the same color.

due to behavioral and/or inherent factors, such as those listed earlier. If the distribution of susceptibilities in a population is given by $n_S(\varepsilon, t)$, shown for an exponential distribution in Figure 1A; then the infection rate is distributed as

$$\hat{r}_I(\varepsilon, t) = \beta I \varepsilon \frac{n_S(\varepsilon, t)}{N_{\text{total}}} \propto \varepsilon \cdot n_S(\varepsilon, t), \quad (2)$$

where N_{total} is the total number of individuals in the population. This distribution, which we refer to as the “draw probability” —that is, the conditional probability that a just-infected individual has susceptibility ε —is shown in Figure 1B, where it is apparent that the mean of the draw probability is higher than the mean of the susceptible pool. This will be true of *any* (non-singular) population distribution, putting downward pressure on the mean. The overall rate of new infections at any time is then

$$r_I = \int_0^\infty \beta I \varepsilon \frac{n_S(\varepsilon, t)}{N_{\text{total}}} d\varepsilon$$

$$r_I = \beta I \bar{\varepsilon} S \quad (\text{any distribution}), \quad (3)$$

where $\bar{\varepsilon}(t)$ is the mean susceptibility of the pool, since $\bar{\varepsilon}(t) = \frac{1}{N_S} \int_0^\infty \varepsilon n_S(\varepsilon, t) d\varepsilon$ with N_S as the total number

of susceptible people in the population. This rate form ($\beta \bar{\varepsilon} I S$) is general; for example, if the entire population has an identical susceptibility of $\varepsilon=1$, (3) simplifies to the classic SIR rate.

In principle, the only constraints on values of ε in $n_S(\varepsilon, t)$ are that $\varepsilon \geq 0$ and that $\bar{\varepsilon}$ is finite; a natural starting point is to assume that susceptibility follows the maximum-entropy distribution (*i.e.*, the least-informative default) under these constraints, which for positive values with a specified mean is the exponential distribution²⁸

$$\frac{n_S(\varepsilon, t)}{N_S} = \frac{e^{-\varepsilon/\bar{\varepsilon}(t)}}{\bar{\varepsilon}(t)}.$$

For this distribution, the draw probability has a mean value of $2\bar{\varepsilon}(t)$ (at any time, provided the distribution remains exponential); that is, the average individual who has just gotten infected was twice as susceptible as the susceptible population as a whole. (All derivations and assumptions not explicitly detailed in this manuscript are contained in the SI.) We can then express how the pool’s average susceptibility $\bar{\varepsilon}$ is affected by the removal of high- ε individuals. Since, on average, the susceptibility of a newly infected individual is $2\bar{\varepsilon}$, the pool’s total susceptibility decreases as $d(\bar{\varepsilon} N_S)/dN_S = 2\bar{\varepsilon}$. Upon integration,

we find the *average* susceptibility of the pool decreases in direct proportion to the number of individuals left in the pool:

$$\bar{\varepsilon}(t) = S(t), \quad (4)$$

(where, without loss of generality, we define the initial population to have $\bar{\varepsilon} = 1$). As a result, the rate of new infections (from (3)) becomes second order in S ,

$$r_I = \beta I S^2 \quad (\text{exponential dist.}).$$

A similar result should be observed by “binning” the susceptibility into discrete levels and introducing a separate ODE for each susceptibility level, as has been employed in previous literature;^{20,29} the match should improve as the number of bins increases, becoming exact at infinite binning. We show the results of numerically integrating such a binned system given an initially exponential susceptibility distribution in Figure 1C. As the number of discrete susceptibility levels is increased, we approach the second-order behavior predicted by this analysis.

The above analysis holds if the distribution is expected to remain exponential throughout the course of the outbreak. Since a distribution will evolve as $\partial n_S(\varepsilon, t)/\partial t = -\beta I \varepsilon n_S(\varepsilon, t)$, then the time-course of the distribution will follow

$$n_S(\varepsilon, t) = n_S(\varepsilon, 0) \cdot e^{-\varepsilon \phi(t)}, \quad (5)$$

where $n_S(\varepsilon, 0)$ is the initial distribution and $\phi(t) \equiv \beta \int_0^t I dt$ is a dimensionless progress variable that is monotonic with time. $\phi(t)$ can be thought of as the cumulative infectious driving force. Therefore, an initially exponential distribution will evolve as

$$n_S(\varepsilon, t) = \frac{N_{\text{total}}}{\bar{\varepsilon}_0} \exp \left\{ - \left(\frac{1}{\bar{\varepsilon}_0} + \phi(t) \right) \cdot \varepsilon \right\},$$

where $\bar{\varepsilon}_0$ is the initial mean. That is, the distribution stays exponential with respect to ε at all times, validating the continued use of the exponential distribution in (4).

Interestingly, we also find that many starting distributions evolve toward an exponential form under the action of contagion. This is shown for a linearly-decreasing distribution in Figure 1D, which we observed via Monte Carlo simulations to tend towards an exponential, through a stochastic sampling process consistent with the draw probability. Indeed, this sculpting behavior can be inferred from (5), which for an initially linearly-decreasing distribution is proportional to $(\varepsilon_{\text{max}} - \varepsilon) \cdot \exp \{ -\phi(t)\varepsilon \}$, where the exponential term becomes dominant as $\phi(t)$ increases.

We can use (5) to describe how contagion sculpts any arbitrary susceptibility distribution. For convenience, we employ the beta distribution, which allows us to craft distributions of characteristic initial shapes, and in Figure 2

we use this distribution to create initial distributions that are longer-tailed (A), bimodal (B), uniform (C), and unimodal (D). Here, we can clearly see how the process of contagion sculpts distributions; features with large ε are quickly diminished; that is, the individuals with high susceptibility to infection are preferentially removed from $n_S(\varepsilon, t)$ at early times. In these sculpting plots, we also show a gamma distribution for reference, with its shape parameter k equal to the a parameter of the beta distribution, and we see that the contagion process sculpts these distributions towards their gamma counterparts. Parts E–H of this figure show the sculpting of gamma distributions, which we see retain their shape during the act of contagion. Indeed, it can be derived that any well-behaved initial distribution—specifically one that is continuous and can be expressed as a power series—will approach a gamma distribution under the sculpting process of (5); we show this in the SI, which also links the beta’s a parameter to the gamma’s k parameter. After a more detailed analysis of the gamma distribution, we will show how the initial distribution shape and the sculpting process interact with the outbreak dynamics.

The gamma distribution is often used to describe variations in susceptibility.^{16,18,20,29} This distribution,

$$\frac{n_S(\varepsilon, 0)}{N_{\text{total}}} = \frac{\varepsilon^{k-1} e^{-\varepsilon/\bar{\varepsilon}_0}}{\left(\frac{\bar{\varepsilon}_0}{k}\right)^k \Gamma(k)},$$

is controlled via a shape parameter k and simplifies to the exponential when $k=1$. If $k < 1$, the gamma becomes a longer-tailed distribution (such as an “80:20” distribution, where 80% of the variation is captured by the most susceptible 20% of the population), and as $k \rightarrow \infty$ the distribution becomes a Dirac delta function. In published studies, k is typically less than one.^{16,18,22,26} As we observed in Figure 2 and formalize in the SI, the gamma distribution is a general solution to the differential equation governing the dynamic sampling process; this makes it an “eigen-distribution” of the force of infection. That is, if a population is initially gamma-distributed it will remain gamma-distributed—with the same shape parameter k and decreasing mean—under the action of (5).

It can be derived that the mean susceptibility, for any given distribution, changes as

$$\frac{d\bar{\varepsilon}}{dS} = \frac{\sigma^2}{\bar{\varepsilon} S} \quad (\text{any distribution})$$

where $\sigma^2(t)$ is the variance of the distribution. Since the variance of the gamma function is $\sigma^2(t) = \bar{\varepsilon}(t)^2/k$ and k stays constant during contagion, it follows that the mean susceptibility scales as

$$\bar{\varepsilon} = S^{1/k} \quad (\text{gamma dist.})$$

for an initial outbreak, giving a rate

$$r_I = \beta I S^{1+\frac{1}{k}} \quad (\text{gamma dist.}).$$

This is exact power-law behavior for gamma-distributed susceptibilities, where the power is given by $p = 1 +$

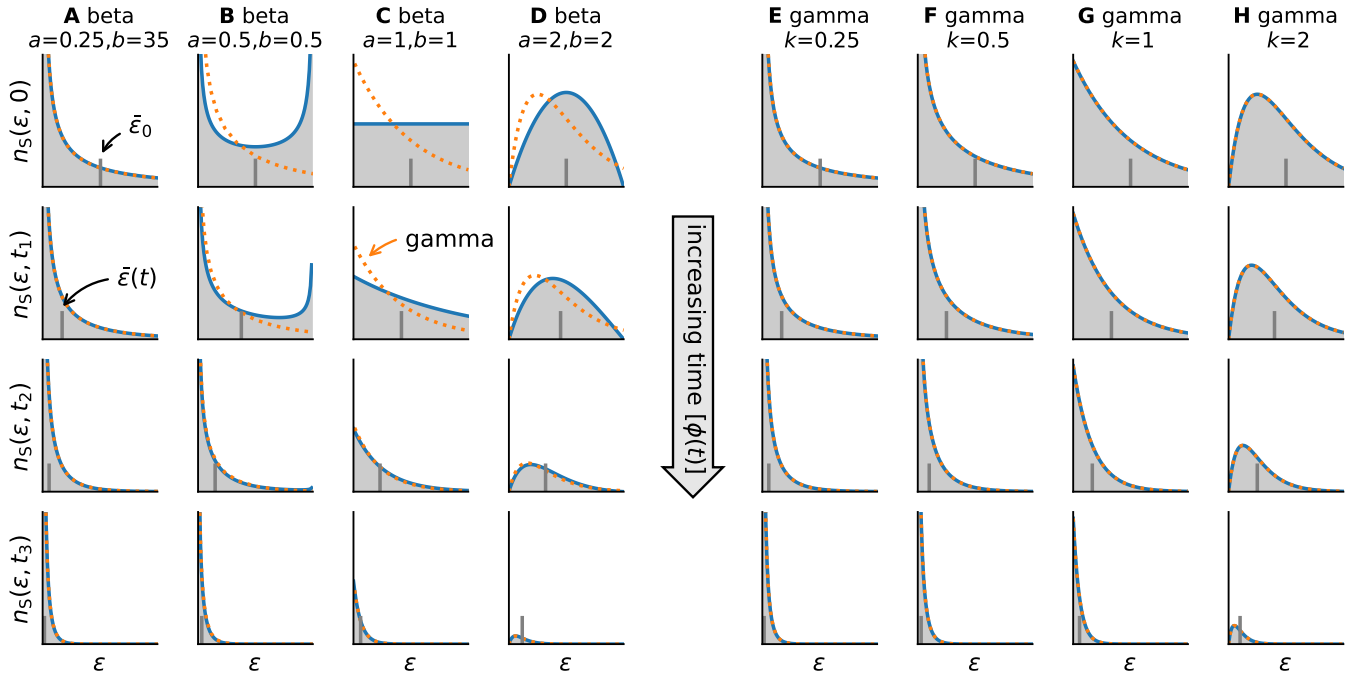


FIG. 2: The sculpting of susceptibility distributions under the act of contagion; that is, by (5). Each column represents the initial distribution indicated at the top of that column, with the shape of that distribution changing with increasing time (tracked by $\phi(t)$) proceeding down the column; at values of $\phi(t) = 0, \frac{1}{2}, 2$, and 4 . In A–D, the orange dashed line shows a gamma function with the same mean and shape parameter $k = a$; in E–H the orange line is included to emphasize that a gamma distribution retains its shape. The small vertical bars indicate $\bar{\epsilon}$, which is set to 1 in all $t = 0$ plots. All plots are scaled identically; that is, all share the same limits on both the abscissa and ordinate.

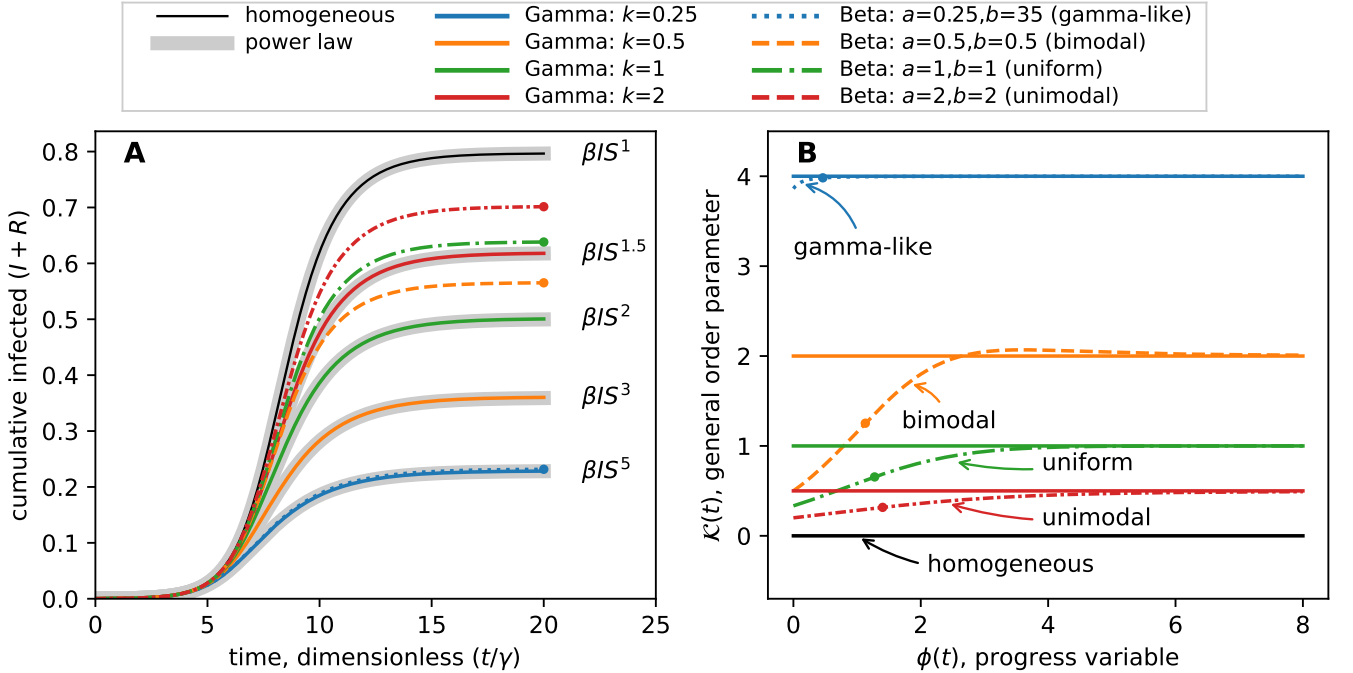


FIG. 3: How the initial susceptibility distribution affects the joint dynamics of infection and distribution sculpting. **A** Infection dynamics for the distributions shown in Figure 2. The gray background curves show power-law models (βIS^p) for comparisons. Time is non-dimensionalized by the recovery rate constant. **B** Effective order parameter $\kappa(t)$ for the same distributions. For the gamma distribution, the order is always $1/k$; for the beta distributions, the order approaches that of a gamma distribution as the sculpting process proceeds. The dot on each beta curve indicates the value at $t/\gamma = 20$. The legend applies to both **A** and **B**.

$1/k$. (Power-law behavior has been suggested elsewhere in models of behavioral change;²¹ here, the behavior emerges naturally from the distribution.) In the case of exponentially-distributed susceptibility ($k=1$), second-order behavior emerges. A longer tail, corresponding to small values of k , can significantly increase the power; for example, the “80:20” distribution ($k \approx 0.25$) pushes the order to approximately five. It is only in the unlikely limit that all individuals are identical ($k \rightarrow \infty$) that we recover the first-order power of the classic SIR model, suggesting the standard SIR model relies on an extreme assumption about variation in susceptibility. This power law provides a convenient framework for capturing the effects of heterogeneous susceptibility through a single additional power-law parameter, which is dictated by the variability of susceptibility.

Next we show how the sculpting process and the outbreak dynamics interact, allowing us to understand how the initial shape of the susceptibility distribution affects the dynamics of disease spread. Conventionally, when outbreak models (*e.g.*, the SIR) are analyzed they are numerically integrated, and when differences in susceptibility are desired this can be achieved by “binning” the susceptibility into many discrete histogram bins,^{20,29} as we did in Figure 1C. However, it is straightforward to track the cumulative progress of the epidemic $\phi(t)$ during the numerical integration. Insofar as we can analytically express the mean susceptibility time course $\bar{\epsilon}(\phi(t))$ for a given initial distribution under the action of (5), we can model outbreak dynamics for arbitrary initial distributions without resorting to the computational expense or complexity involved with binning. We give full details of how this can be simply implemented in the SI. We note that methods have been introduced in prior literature to integrate such a system without binning, notably a method that approximates the partial differential equation as a truncated set of ordinary differential equations involving the moments of the distribution, making subsequent assumptions about relationships between these moments.^{16,32,33} In contrast, the method here gives an exact solution, shows precisely when assumptions about moment relationships hold, and does so without expanding the number of differential equations, relative to the standard SIR model. We have performed this integration for the initial distributions shown in Figure 2, and the results are shown in Figure 3A. Here, we see an orderly progression among the gamma distributions, with the longer-tailed distributions exhibiting reduced final outbreak size; further, we see that the gamma and beta distributions whose initial shape is nearly indistinguishable (gamma, $k = 0.25$ with beta, $a = 0.25, b = 35$) behave almost indistinguishably. As expected, the gamma distributions follow the power-law relations exactly. As is apparent, the longer the tail on the distribution, the more suppressed the size of the outbreak, as the initially high rate is caused by those with abnormally high susceptibilities.

While we have only analytically derived a power law

for gamma distributions, relating $\bar{\epsilon}$ to S^p , for other distributions we can define an instantaneous order parameter $\mathcal{K}(t)$ as

$$\mathcal{K}(t) \equiv \frac{d(\ln \bar{\epsilon})}{d(\ln S)}$$

which allows us to understand the deviation from such a law, and can inform us how the contagion process sculpts the susceptibility distribution. For gamma distributions, $\mathcal{K}(t) = 1/k$ at all times. We provide an expression for $\mathcal{K}(t)$ in terms of $\phi(t)$ for the beta distribution in the SI, and in Figure 3B we show how $\mathcal{K}(t)$ changes for the beta distributions. We see that instantaneous orders of the beta distributions tend towards the orders of the corresponding gamma distributions. That is, the contagion process sculpts the beta distributions towards gamma distributions, and as this happens the order approaches the constant order of the gamma distribution. How this affects the outbreak behavior depends upon the relevant timescales of the sculpting process versus that of the infection dynamics.

For the beta distribution at $a = \frac{1}{4}$, $b = 35$, which very closely resembles a gamma distribution, we see that the order starts at approximately 4 and closely follows the behavior of the corresponding ($k=4$) gamma distribution. This was also apparent from the numerical integration of these two starting distributions, which give nearly indistinguishable results. That is, if the initial distribution can be reasonably approximated by a gamma distribution, then we can expect the power-law behavior to describe well the dynamics. For the more extreme initial distributions, such as the bimodal or uniform, we see that $\mathcal{K}(t)$ changes much more dramatically over the course of the outbreak. Although they approach a gamma distribution at large values of $\phi(t)$, in practice these $\phi(t)$ values may never be reached, as the outbreak may reach its final size before the sculpting process can asymptote. We see precisely this for the bimodal and uniform distributions, where the dot on the $\mathcal{K}(t)$ figures shows the value of $\mathcal{K}(t)$ at a time when the epidemic has, in effect, concluded. Finally, we see the unimodal distribution has a relatively low order parameter, which we expect, as this most closely resembles the implied homogeneous assumption of the classic SIR model, for which $\mathcal{K}(t) = 0$ at all times.

How does a power-law dependence of the infection rate affect epidemic model predictions? First, we note that in the early, exponential-like growth phase of an outbreak—when most of the pre-emptive measures are decided—the models are indistinguishable (since $S \approx 1$, then $S^p \approx 1$). This means that when the model parameters are fit in this exponential-like growth phase, the estimate of β (or alternatively $\mathcal{R}_0 \equiv \beta/\gamma$) will be identical in each model (see Figure 4A). A deviation in the dynamics of the different models appears given sufficient depletion of susceptibles (see Figure 4B). Assuming the epidemic proceeds in a naïve population, the final size under a 2nd-order

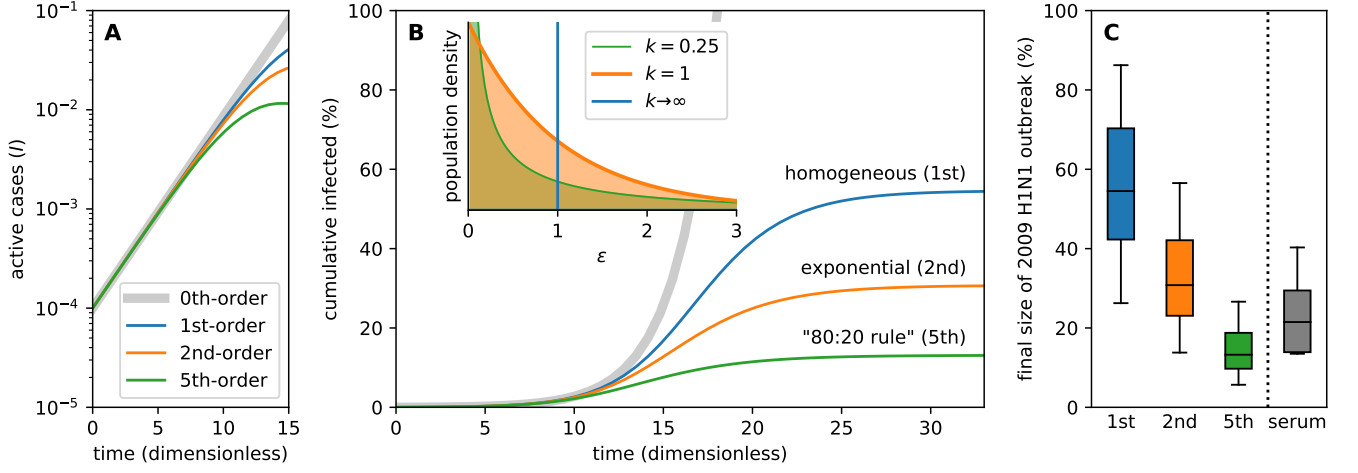


FIG. 4: Outbreak dynamics and model comparison to the 2009 H1N1 outbreak. **A:** The higher-order models are indistinguishable from one another in the early, exponential-like region (marked as “0th-order”), where the models are frequently parameterized. **B:** Outbreak progression with various assumed susceptibility distributions. The inset shows a gamma distribution at different k values. In all models, $\beta/\gamma (= \mathcal{R}_0)$ is set to 1.47, the median value estimated from 78 studies at the early stages of the 2009 H1N1 outbreak,³⁰ and time is non-dimensionalized by the recovery rate ($\gamma \cdot t$). **C:** Final size predictions based on the 78 \mathcal{R}_0 values measured³⁰ at early stages of the infection, in the 1st-, and 2nd-, and 5th-order models, compared with 11 seroepidemiological measurements obtained³¹ after the outbreak stabilized.

model is predicted to be

$$Z = 1 - \frac{1}{\mathcal{R}_0} \quad (2\text{nd order}).$$

For 1st- and p th-orders, implicit algebraic equations are given in the SI. Figure 4B shows that there can be very substantial differences between final size predictions when comparing the conventional SIR model with predictions from models with intrinsic variation in susceptibility. We note that these results agree with predictions made elsewhere that heterogeneity reduces the predicted severity of the outbreak.^{21,24–26} Within the power-law model, the herd-immunity threshold is predicted to be

$$p_C = 1 - \frac{1}{\mathcal{R}_0^{1/p}}.$$

These herd-immunity and final-size analyses are only meaningful when the population’s immunity is accrued naturally through the dynamics of the outbreak itself; if immunity is acquired through vaccinations applied randomly, then the final-size and herd-immunity estimates will tend toward the classic SIR predictions.

Differences in final-size predictions when including risk heterogeneity as compared to those from conventional SIR models can be relevant to real-world outbreaks, as we examine for the 2009 H1N1 influenza outbreak, where initial estimates of the final outbreak size were reportedly much higher than occurred in practice.³¹ In Figure 4B, we compare the power-law behavior using models parameterized with the mean \mathcal{R}_0 estimated at the early stages of the outbreak.³¹ In the included bar chart (Figure 4C),

we compare model predictions using 78 published estimates of \mathcal{R}_0 (from different locales)³⁰ to final-size measurements based on 11 serological studies.³¹ We observe that the higher-order models are more consistent with the final-size measurements. It is not uncommon for models to over-predict the ultimate size of epidemics,^{31,34,35} although we note that non-pharmaceutical interventions such as social distancing are expected to reduce this final size,^{1,36} even after being later relaxed. While predicting final outbreak sizes based on initial measurements is challenging, the significant improvement of the higher-order models lends credence to the importance of accounting for heterogeneity in the susceptibility of naïve populations.

There are other factors worth considering in this analysis. First, this framework does not assume any correlation between spreading propensity and infection susceptibility, so that super-spreaders appear with a frequency identical to their prevalence in the population. It seems plausible that many of the social traits that contribute to higher susceptibility would also lead to higher spreading. If a positive correlation exists between spreading and susceptibility, then the “super-spreaders” will be most active at the beginning of an outbreak and contribute disproportionately to the rate of infection, but as the outbreak progresses, they also will be disproportionately removed early, causing more downward pressure on the relative rate of infection. The analysis also assumes that the susceptibility of each individual in the population is static over the timescales relevant to the outbreak, so that an individual does not become more or less susceptible at any point, and that there is no societal response. If these changes to susceptibility are random, this would decrease the effect suggested here; however, if they are behavior

responses, it may increase the effect.²¹

Overall, this study outlines that quantifying and accounting for variability in susceptibility are critical to designing effective policies. When we account for heterogeneity in infection susceptibility, the rate equation of the standard SIR model follows a generic power law with an exponent that increases with the variance and tends toward second-order behavior for an exponential susceptibility distribution. Other starting distributions can be integrated with negligible computational cost or

complexity by relating $\bar{\varepsilon}$ to $\phi(t)$. This provides a principled route to account for variability in human populations that are implicitly neglected in classic epidemiological models. The new framework adds negligible computational cost, facilitating integration with more complex models. More critically, the analysis reveals that assessing the joint dynamics of the susceptibility distribution can have drastic consequences on naturally-acquired herd immunity predictions, highlighting the importance of quantifying susceptibility variance for COVID-19 and other infectious diseases.

-
- * jsweitz@gatech.edu
 † andrew.peterson@brown.edu
- ¹ Bjørnstad, O.N.; Shea, K.; Krzywinski, M.; Altman, N. Modeling infectious epidemics. *Nat. Methods* **2020**; *17*, 455–456.
 - ² Kermack, W.O.; McKendrick, A.G. A contribution to the mathematical theory of epidemics. *Proc. R. Soc. London. A* **1927**; *115*, 700–721.
 - ³ Anderson, R.M.; May, R.M. *Infectious Diseases of Humans: Dynamics and Control*. Oxford University Press **1992**.
 - ⁴ Keeling, M.J.; Rohani, P. *Modeling Infectious Diseases in Humans and Animals*. Princeton University Press, 1st edition edition **2007**.
 - ⁵ Bertozzi, A.L.; Franco, E.; Mohler, G.; Short, M.B.; Sledge, D. The challenges of modeling and forecasting the spread of COVID-19. *Proc. Nat. Acad. Sci. USA* **2020**; *117*, 16732–16738.
 - ⁶ Moghadas, S.M.; Fitzpatrick, M.C.; Sah, P.; Pandey, A.; Shoukat, A.; Singer, B.H.; Galvani, A.P. The implications of silent transmission for the control of COVID-19 outbreaks. *Proc. Nat. Acad. Sci. USA* **2020**; *117*, 17513–17515.
 - ⁷ Wilson, E.B.; Worcester, J. The Law of Mass Action in Epidemiology. *Proceedings of the National Academy of Sciences* **1945**; *31*, 24–34.
 - ⁸ Liu, W.; Levin, S.A.; Iwasa, Y. Influence of nonlinear incidence rates upon the behavior of SIRS epidemiological models. *Journal of Mathematical Biology* **1986**; *23*, 187–204.
 - ⁹ Liu, W.; Hethcote, H.W.; Levin, S.A. Dynamical behavior of epidemiological models with nonlinear incidence rates. *Journal of Mathematical Biology* **1987**; *25*, 359–380.
 - ¹⁰ Hethcote, H.W.; van den Driessche, P. Some epidemiological models with nonlinear incidence. *Journal of Mathematical Biology* **1991**; *29*, 271–287.
 - ¹¹ Regoes, R.R.; Ebert, D.; Bonhoeffer, S. Dose-dependent infection rates of parasites produce the Allee effect in epidemiology. *Proceedings of the Royal Society of London. Series B: Biological Sciences* **2002**; *269*, 271–279.
 - ¹² Chowell, G.; Sattenspiel, L.; Bansal, S.; Viboud, C. Mathematical models to characterize early epidemic growth: A review. *Physics of Life Reviews* **2016**; *18*, 66–97.
 - ¹³ Longini, I.M.; Halloran, M.E. A Frailty Mixture Model for Estimating Vaccine Efficacy. *Applied Statistics* **1996**; *45*, 165.
 - ¹⁴ Halloran, M.E.; Longini, I.M.; Struchiner, C.J. Estimation and Interpretation of Vaccine Efficacy Using Frailty Mixing Models. *American Journal of Epidemiology* **1996**; *144*, 83–97.
 - ¹⁵ Woolhouse, M.E.J.; Dye, C.; Etard, J.F.; Smith, T.; Charlwood, J.D.; Garnett, G.P.; Hagan, P.; Hii, J.L.K.; Ndhlovu, P.D.; Quinnell, R.J.; Watts, C.H.; Chandiwana, S.K.; Anderson, R.M. Heterogeneities in the transmission of infectious agents: Implications for the design of control programs. *Proc. Nat. Acad. Sci. USA* **1997**; *94*, 338–342.
 - ¹⁶ Dwyer, G.; Elkinton, J.S.; Buonaccorsi, J.P. Host Heterogeneity in Susceptibility and Disease Dynamics: Tests of a Mathematical Model. *Am. Nat.* **1997**; *150*, 685–707.
 - ¹⁷ Dwyer, G.; Dushoff, J.; Elkinton, J.S.; Levin, S.A. Pathogen-Driven Outbreaks in Forest Defoliators Revisited: Building Models from Experimental Data. *The American Naturalist* **2000**; *156*, 105–120.
 - ¹⁸ Smith, D.L.; Dushoff, J.; Snow, R.W.; Hay, S.I. The entomological inoculation rate and Plasmodium falciparum infection in African children. *Nature* **2005**; *438*, 492–495.
 - ¹⁹ Izhar, R.; Ben-Ami, F. Host age modulates parasite infectivity, virulence and reproduction. *Journal of Animal Ecology* **2015**; *84*, 1018–1028.
 - ²⁰ King, J.G.; Souto-Maior, C.; Sartori, L.M.; de Freitas, R.M.; Gomes, M.G.M. Variation in Wolbachia effects on Aedes mosquitoes as a determinant of invasiveness and vectorial capacity. *Nat. Commun.* **2018**; *9*, 1483.
 - ²¹ Eksin, C.; Paarporn, K.; Weitz, J.S. Systematic biases in disease forecasting – The role of behavior change. *Epidemics* **2019**; *27*, 96–105.
 - ²² Corder, R.M.; Ferreira, M.U.; Gomes, M.G.M. Modelling the epidemiology of residual Plasmodium vivax malaria in a heterogeneous host population: A case study in the Amazon Basin. *PLoS Comput. Biol.* **2020**; *16*, e1007377.
 - ²³ Endo, A.; Abbott, S.; Kucharski, A.J.; and, S.F. Estimating the overdispersion in COVID-19 transmission using outbreak sizes outside China. *Wellcome Open Research* **2020**; *5*, 67.
 - ²⁴ Britton, T.; Ball, F.; Trapman, P. A mathematical model reveals the influence of population heterogeneity on herd immunity to SARS-CoV-2. *Science* **2020**; In press, DOI:10.1126/science.abc6810.
 - ²⁵ Hébert-Dufresne, L.; Althouse, B.M.; Scarpino, S.V.; Al-lard, A. Beyond R_0 : Heterogeneity in secondary infections and probabilistic epidemic forecasting. *ArXiv* **2020**; 2002.04004.
 - ²⁶ Gomes, M.G.M.; Corder, R.M.; King, J.G.; Langwig, K.E.; Souto-Maior, C.; Carneiro, J.; Goncalves, G.; Penha-

- Goncalves, C.; Ferreira, M.U.; Aguas, R. Individual variation in susceptibility or exposure to SARS-CoV-2 lowers the herd immunity threshold. *medRxiv* **2020**; 2020.04.27.20081893.
- ²⁷ Bansal, S.; Grenfell, B.T.; Ancel Meyers, L. When individual behaviour matters: homogeneous and network models in epidemiology. *Journal of The Royal Society Interface* **2007**; 4, 879–891.
- ²⁸ Jaynes, E.T. *Probability Theory*. Cambridge University Press **2003**.
- ²⁹ Langwig, K.E.; Wargo, A.R.; Jones, D.R.; Viss, J.R.; Rutan, B.J.; Egan, N.A.; Sá-Guimarães, P.; Kim, M.S.; Kurath, G.; Gomes, M.G.M.; Lipsitch, M. Vaccine Effects on Heterogeneity in Susceptibility and Implications for Population Health Management. *mBio* **2017**; 8, e00796–17.
- ³⁰ Biggerstaff, M.; Cauchemez, S.; Reed, C.; Gambhir, M.; Finelli, L. Estimates of the reproduction number for seasonal, pandemic, and zoonotic influenza: a systematic review of the literature. *BMC Infect. Dis.* **2014**; 14, 480.
- ³¹ Nishiura, H.; Chowell, G.; Castillo-Chavez, C. Did Modeling Overestimate the Transmission Potential of Pandemic (H1N1-2009)? Sample Size Estimation for Post-Epidemic Seroepidemiological Studies. *PLoS ONE* **2011**; 6, e17908.
- ³² Dushoff, J. *Effects of host heterogeneity in epidemic models*. Ph.D. thesis, Princeton University **1996**.
- ³³ Dushoff, J. Host Heterogeneity and Disease Endemicity: A Moment-Based Approach. *Theoretical Population Biology* **1999**; 56, 325–335.
- ³⁴ Butler, D. Models overestimate Ebola cases. *Nature* **2014**; 515, 18–18.
- ³⁵ King, A.A.; de Cellès, M.D.; Magpantay, F.M.G.; Rohani, P. Avoidable errors in the modelling of outbreaks of emerging pathogens, with special reference to Ebola. *Proc. R. Soc. B* **2015**; 282, 20150347.
- ³⁶ Ma, J.; Earn, D.J.D. Generality of the Final Size Formula for an Epidemic of a Newly Invading Infectious Disease. *Bull. Math. Biol.* **2006**; 68, 679–702.